Deformation modes and ideal strengths of ternary layered Ti_2AlC and Ti_2AlN from first-principles calculations

Ting Liao,[1,2] Jingyang Wang,[1,3] and Yanchun Zhou[1]
[1]*Shenyang National Laboratory for Materials Science, Institute of Metal Research, Chinese Academy of Sciences, Shenyang 110016, China*
[2]*Graduate School of Chinese Academy of Sciences, Beijing 100039, China*
[3]*International Centre for Materials Physics, Institute of Metal Research, Chinese Academy of Sciences, Shenyang 110016, China*

(Received 7 July 2005; revised manuscript received 7 March 2006; published 14 June 2006)

Deformation and failure modes were studied for Ti_2AlC and Ti_2AlN by deforming the materials from elasticity to structural instability using the first-principles density functional calculations. We found that the $TiC_{0.5}/TiN_{0.5}$ slabs remain structurally stable under deformations, whereas the weak Ti-Al bonds accommodate deformation by softening and breaking at large strains. The structural stability of the ternary compound is determined by the strength of Ti-Al bond, which is demonstrated to be less resistive to shear deformation than to tension. The ideal stress-strain relationships of ternary compounds are presented and compared with those of the binary materials, TiC and TiN, respectively. For Ti_2AlC and Ti_2AlN, their ideal tensile strengths are comparable to those of the binary counterparts, while the ideal shear strengths yield much smaller values. Based on electronic structure analyses, the low shear deformation resistance is well interpreted by the response of weak Ti-Al bonds to shear deformations. We propose that the low shear strengths of Ti_2AlC and Ti_2AlN originate from low slip resistance of Al atomic planes along the basal plane, and furthermore suggest that this is the mechanism for low hardness, damage tolerance, and intrinsic toughness of ternary layered carbides and nitrides.

DOI: 10.1103/PhysRevB.73.214109 PACS number(s): 62.20.−x, 71.20.−b, 81.05.Je

I. INTRODUCTION

Ceramics are typically intrinsically brittle and are sensitive to microscopic cracks. Ceramic matrix composites (CMC) with controlled interfaces have shown much improved toughness and strength as reported by Lawn *et al.*[1] They provided a generalized method to enhance toughness by controlling microstructural characteristics of CMC, and hence to increase damage-tolerant capability by certain energy dissipating mechanisms.

For sameness, easy bond-breaking events involving failure of weak interplanar bonds might serve as energy absorption mechanism for single crystalline. Intrinsic damage tolerance can be achieved in materials with special crystal structures, such as layered compounds. Recently, the ternary layered carbides and nitrides have attracted attention due to their unique properties combining merits of both metals and high-performance ceramics. The properties can be traced to high modulus, easy machinability, good damage tolerance, and microscale ductility at room temperature, as well as the excellent thermal shock resistance and high temperature oxidation resistance, etc.[2] These ternary layered compounds yielded a common formula of $T_{n+1}AX_n$ (where T is an early transition metal, A is an A-group element, and X is carbon and/or nitrogen), and crystallized with space group $P6_3/mmc$. The crystal structure of $T_{n+1}AX_n$ compounds can be described as slabs of nonstoichiometric transition metal carbides or nitrides being interleaved and mirrored by close-packed atomic planes of A-group elements. It was assumed that the weak coupling between the transition metal carbide and/or nitride slabs and A-group element atomic planes might be responsible for the unique mechanical properties.[3] To date, no explanation has been proposed for this hypothesis. Moreover, the deformation mechanism of $T_{n+1}AX_n$ compound was still unclear in an atomistic scale, and it is therefore impossible to state the physical origin of intrinsic damage tolerance.

Theoretical investigations have been conducted to elastic stiffness of $T_{n+1}AX_n$ compound in the past several years.[4–6] However, the origin of damage tolerance and low hardness was far from clarified, because these macroscopic mechanical properties are determined by the upper bound of chemical bonds at a large strain. Therefore, investigations should be focused on deformation mechanism up to structural instability. Many theoretical works have been done to study the structural stability, failure modes, and ideal strengths of metals and ceramics.[7–11] In these studies, the experimental strengths of materials were well interpreted and predicted by examining the ideal deformation modes, as well as the ideal stress-strain relationships. Furthermore, as fundamental physical property of material against structural failure, the ideal strengths therein were comprehensively discussed for both tensile and shear deformations.

We studied two representative ternary layered compounds, Ti_2AlC and Ti_2AlN, in the present investigation. These compounds are typical ternary layered $T_{n+1}AX_n$ phases, which show capability of damage tolerance and intrinsic toughness at room temperature. For comparison, binary compounds TiC and TiN were also studied following the same method proposed in the pioneer work of Jhi *et al.*[12] Although calculations on elastic limits of a solid are computationally consuming, particularly when the strained solid has low symmetry, it is possible to study the ideal stress-strain relationships and atomistic deformation modes with

the help of state-of-the-art first-principles computation.[13]

The present paper is organized as follows. The computational details are described in Sec. II. In Sec. III we present results of theoretical stress-strain relationships of Ti_2AlC, Ti_2AlN, TiC, and TiN under tensile and shear deformations. Atomistic deformation modes and the electronic structure analysis are also discussed. The conclusions are summarized in Sec. IV.

II. COMPUTATIONAL DETAILS

The equilibrium crystal parameters and ground-state electronic structure were calculated using the CASTEP[13] code, in which the plane-wave pseudopotential total-energy calculation was performed. Interactions of electrons with ion cores were represented by the Vanderbilt-type ultrasoft pseudopotential for Ti, Al, C, and N atoms. The electronic exchange-correlation energy was treated under the generalized gradient approximation (GGA-PW91).[14] The plane-wave basis set cutoff was set as 450 eV for all cases, which was sufficient in leading to good convergence for total energy and forces acting on the atoms. The special points sampling integration over the Brillouin zone was employed by using the Monkhorst-Pack method with $6\times6\times6$ and $10\times10\times2$ special k-point meshes for binary and ternary crystals, respectively. The tolerances for the geometry optimization were selected as the difference in total energy within 5.0×10^{-6} eV/atom, the maximum ionic Hellmann-Feynman force within 0.01 eV/Å, the maximum ionic displacement within 5.0×10^{-4} Å, and the maximum stress within 0.02 GPa. Increasing the plane-wave cutoff energy to 700 eV and the k-point meshes to $8\times8\times8$ and $14\times14\times2$ changed the total energy and lattice constants by less than 0.005 eV/ atom and 0.02%, respectively. Therefore, the present computations were precise enough to represent the ground-state properties of both binary and ternary compounds.

Deformation and failure modes were studied in the present paper. Tensile and shear deformations were applied with a series of strains ε along selected easy deformation paths. Tensile deformation was performed along the [001] direction for both ternary and binary ceramics. Uniaxial tension were also conducted in the [110] and [111] directions for binary compounds. The maximum stresses achieved for [110] and [111] tensions are larger than the value for [001] tension. The [0001](0001) tension was selected because Ti_2AlC and Ti_2AlN have layered hexagonal crystal structure. To ensure that the material was under a uniaxial stress state, relaxation of the structure perpendicular to the applied strain direction was performed by holding the applied strain fixed and adjusting the other two normal strain components independently until the calculated Hellmann-Feynman stresses were both less than 0.1 GPa.

For the shear deformation path, different strain modes were chosen for binary and ternary compounds. For binary crystals, the $[1\ \bar{1}\ 0](110)$ slip system was reported to be the primary slip system of rock-salt-structured transition metal carbides and nitrides at low temperatures.[15] Therefore, a series of incremental shear strains were applied in the $[1\bar{1}0]$ direction on the (110) plane. For ternary compounds with hexagonal symmetry, the slip systems, which could be activated during loading, were quite limited in Ti_2AlC and Ti_2AlN. Perfect dislocations were detected lying on the (0001) basal planes with a Burgers vector of $b=1/3\langle11\bar{2}0\rangle$ by transmission electron microscopy after a deformation at room-temperature.[16,17] Since only basal-plane slip is preferred in Ti_2AlC and Ti_2AlN, we studied the deformation modes along the $[1\bar{2}10]$ (0001) shear path for ternary compounds.

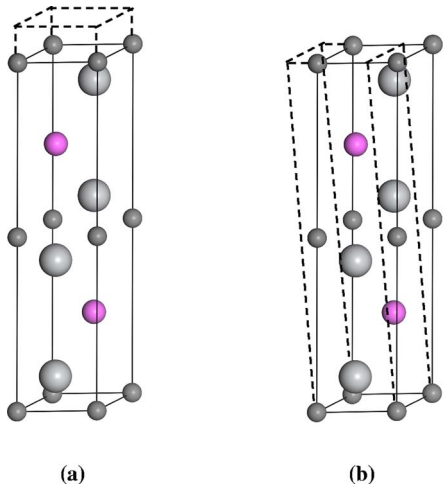

FIG. 1. (Color online) Schematic illustration of (a) [0001](0001) tension and (b) $[1\bar{2}10](0001)$ shear deformation of ternary compound.

III. RESULTS AND DISCUSSION

A. Ideal stress-strain curves

Firstly, the unit cell of ternary compounds were strained following the [0001](0001) tensile and $[1\bar{2}10](0001)$ shear paths, as schematically illustrated in Fig. 1. Stresses were calculated thereafter for materials being deformed from elasticity to structural instability. For comparison, the stress-strain curves of binary TiC and TiN under tensile and shear deformations were also examined. In Fig. 2, we display the strain dependences of Hellmann-Feynman stresses for TiC, TiN, Ti_2AlC, and Ti_2AlN.

The data of tensile stress versus strain is presented by empty triangles in Fig. 2. For binary compounds, the tensile stresses increase more abruptly than those of Ti_2AlC and Ti_2AlN, by which shows a higher elastic moduli than the latter ternary compounds.[4,18] The maximum tensile stresses, defined as the ideal tensile strength, are 33 GPa, 30 GPa, 25 GPa, and 28 GPa for TiC, TiN, Ti_2AlC, and Ti_2AlN, respectively. It is noted that the ideal tensile strengths of ternary compounds are slightly lower than those of the binary counterparts. Compared to those of TiC and TiN, the tensile strengths decrease by 8 GPa and 2 GPa for Ti_2AlC and Ti_2AlN, respectively.

As reported by Jhi *et al.*, numerical fluctuation on lattice freedoms was important for structural relaxation of binary

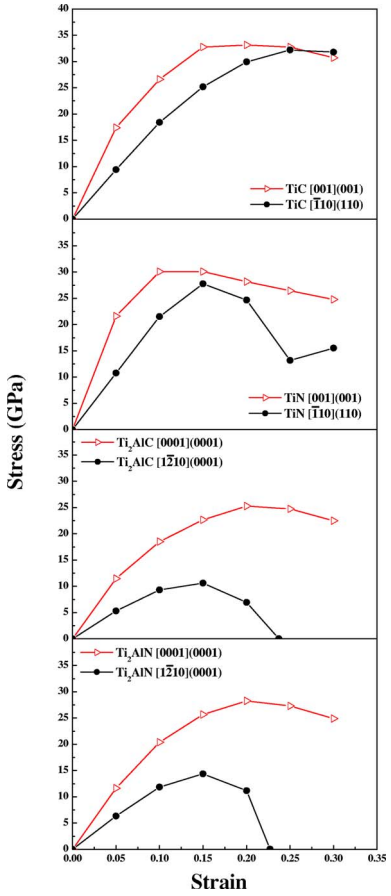

FIG. 2. (Color online) Induced Hellmann-Feynman stresses (in GPa) as a function of applied strain for (a) TiC, (b) TiN, (c) Ti_2AlC, and (d) Ti_2AlN. Empty triangles represent the tensile stresses under uniaxial tension along the z axis, while the solid circles correspond to the shear stresses derived from shear deformations in $(110)[\bar{1}10]$ and $(0001)[1\bar{2}10]$ slip systems for binary and ternary compounds, respectively. Solid lines are guides for the eye.

TiC and TiN under shear deformation.[12] To achieve stable lattice configuration under shear strain, we followed the same optimization procedures described in Ref. 12. Internal freedom fluctuations were applied to the strained lattice, and then a stable configuration on the energy surface was obtained. For TiN under shear strains beyond 0.15, similar to the result reported in Ref. 12, a lattice configuration with lower total energy was obtained by the N atom undergoing a spontaneous shift from its original position to a new position along the (110) plane. As a result, a discontinuity in the stress-strain curve was observed. In contrast to TiN, TiC does not undergo such a symmetry-broken event when the same optimization procedure was conducted. By performing perturbation on internal degrees of freedom, the obtained results for binary compounds were in good agreement with the results reported in Ref. 12. Furthermore, we also applied a series of internal freedom perturbations to the ternary compounds, and the strained cell converged to the same lattice configuration.

The solid circles in Figs. 2(a) and 2(b) represent the shear stresses for binary compounds under $[\bar{1}10](110)$ shear deformations. The ideal shear strengths are 32 GPa and 28 GPa for TiC and TiN, respectively. These shear strengths of binary compounds are comparable to the corresponding ideal tensile strengths. The stress-strain curve of TiC remains smooth throughout the shear strain path. In contrast, a discontinuity is identified for the stress-strain curve of TiN. The origin for discontinuity has been clearly outlined by Jhi *et al.* using the pseudopotential density functional total-energy method.[12] Therein, the ideal shear strengths of TiC and TiN were reported as 35 GPa and 31 GPa, respectively. A good agreement was achieved between the present study and previous calculation.

TABLE I. Computed ideal tensile strengths σ and shear strengths τ (in GPa) of TiC, TiN, Ti_2AlC, and Ti_2AlN, together with computed bulk modulus B, shear modulus G, and elastic constant c_{44} (in GPa). The experimental Vickers hardnesses (in GPa) are also included.

	B	G	c_{44}	σ	τ	Hardness[a]
TiC	253	166	160	33	32	29
TiN	281	252	193	30	28	21
Ti_2AlC	137	117	111	25	11	4.5
Ti_2AlN	156	117	130	28	14	4

[a]References 19–21

The stress-strain curves display noticeable low values for Ti_2AlC and Ti_2AlN under $[1\bar{2}10](0001)$ shear deformations, as shown in Figs. 2(c) and 2(d). These curves locate below those for tension, and therefore, low shear strengths are obtained. The ideal shear strength of Ti_2AlC is about one third of that of TiC, and the value is half for Ti_2AlN compared with that of TiN.

The ideal strengths of studied compounds are tabulated in Table I, together with the calculated bulk modulus B, shear modulus G, elastic constant c_{44}, and the experimental Vickers hardness.[19–21] The ideal tensile strengths change slightly and show no obvious difference between binary and ternary compounds. On the other hand, the ideal shear strength shows a similar trend with hardness. Low Vickers hardness of ternary compounds is suggested to originate from the low resistance to shear deformation. As known, hardness measurements test the resistance of a material to permanent plastic deformation. For strong covalently bonded materials, such as binary transition metal carbide and nitride, the low mobility of dislocation is determined by the very high bond-breaking energy at a large shear strain. Such low dislocation mobility can also be quantitatively evaluated from a high Peierls stress or the stress required moving a dislocation one atomic Burgers vector. Using the calculated lattice and mechanical parameters, we estimated the maximum value of Peierls shear stress to initiate the movement of a dislocation on glide planes of TiC, TiN, Ti_2AlC, and Ti_2AlN by[22]

$$\sigma_s = \frac{2G}{1-\nu}\exp\left(-\frac{2\pi\lambda}{b}\right), \tag{1}$$

where $\lambda=[(3-2\nu)/4(1-\nu)]d$, G is the shear modulus, b the Burgers vector, d the spacing between slip planes, and υ the Poisson's ratio.

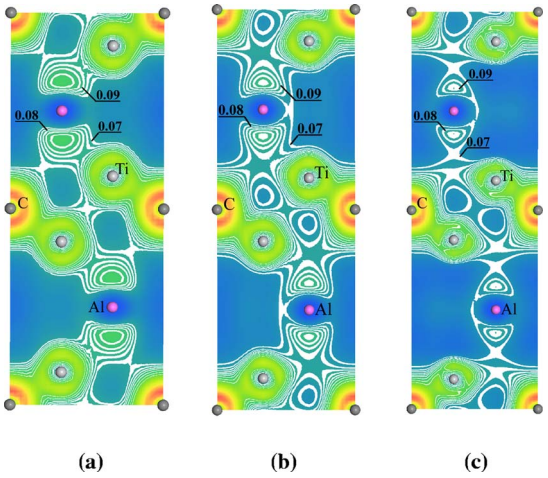

FIG. 3. (Color online) Distribution of valence electron density in a $(11\bar{2}0)$ plane of Ti_2AlC at various tensile deformations along the z axis: (a) unstrained, (b) 0.1 tensile strain, and (c) 0.2 tensile strain.

Formula (1) deduces the relative magnitude of maximum Peierls stresses for binary and ternary compounds. The calculated σ_s of Ti_2AlC and Ti_2AlN are only 21% and 13% of the σ_s of TiC and TiN, respectively. The lower Peierls stresses of Ti_2AlC and Ti_2AlN seem to suggest that dislocations are more active in the ternary compounds. However, based on transmission electron microscope investigation, dislocations in ternary layered carbide are observed to be constrained to the basal plane and contribute little to the room-temperature plastic deformation.[16] Instead, intrinsic toughness and ductility originates from processes like cleavage, delamination, buckling, and kinking.[23] There are two factors determining the experimental strength of a material. One is the curvature of the energy barrier (the elastic modulus) and the other is the height of the energy barrier, which corresponds to the ideal strength. Ternary layered carbide/nitride shows both low shear moduli and theoretical shear strengths, and therefore yields low resistance for shear-induced structural instability. The low hardness of Ti_2AlC and Ti_2AlN can be best understood by an easy basal plane slip derived from weak coupling between $TiC_{0.5}/TiN_{0.5}$ slabs and Al atomic layers. As a result, these Al-containing carbide and nitride are soft and damage tolerant.

B. Deformation mode under tension

Deformation mode for applied [0001](0001) tension was studied in order to gain a deeper insight into the failure of ternary layered compound. Figure 3 presents slices of valence electron density distribution in a $(11\bar{2}0)$ atomic plane of Ti_2AlC under [0001](0001) tensile strains. It shows that the Ti-Al bonds are perturbed more significantly than the Ti-C bonds. The inhomogeneous bond-relaxation for Ti-C and Ti-Al bonds originates from different covalent bonding strengths.[3] The Ti-Al bond weakens significantly under increased uniaxial tension, and leads to the stress relaxation.

In Fig. 4, we illustrate the electron density difference, which shows rearrangement of valence electrons under applied tension. One may notice that the strong Ti-C covalent bonds are quite stable. On the other hand, the electron density distribution of Ti-Al bonds undergoes dramatic changes. Accompanied with stretching of Ti-Al bonds, the electron density corresponding to Ti $d(e_g)$-Al p bond exhibits an obvious depletion at applied tensile strain of 0.2. As a result, the stress reaches maximum value, and the material experiences a critical point to failure. After Ti-Al bond breaks, the electron density obviously accumulates along the Ti-$d(e_g)$ orbitals. The features are the same for Ti_2AlN under tensile deformation, which is not presented for briefness.

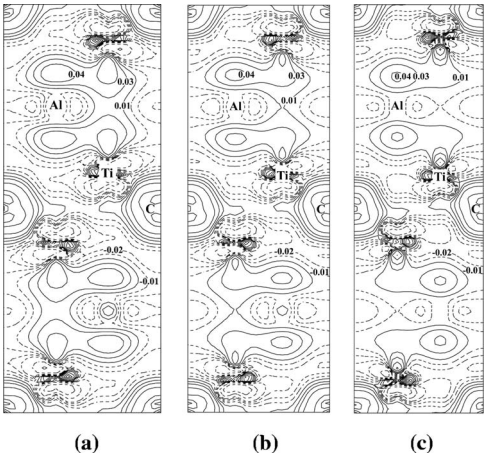

FIG. 4. Electron density difference in a slice of $(11\bar{2}0)$ atomic plane of Ti_2AlC: (a) unstrained, (b) 0.1 tensile strain, and (c) 0.2 tensile strain.

C. Deformation mode under shear strain

Figure 5 shows slices of valence electron density distribution in a $(11\bar{2}0)$ atomic plane of Ti_2AlC under $[1\bar{2}10](0001)$ shear strains. When Ti_2AlC is shear deformed, Al atoms slip smoothly along the basal plane, and only half of the Ti-Al bonds stretch and soften gradually according to the applied strain mode. In contrast, the strong Ti-C covalent bonds re-

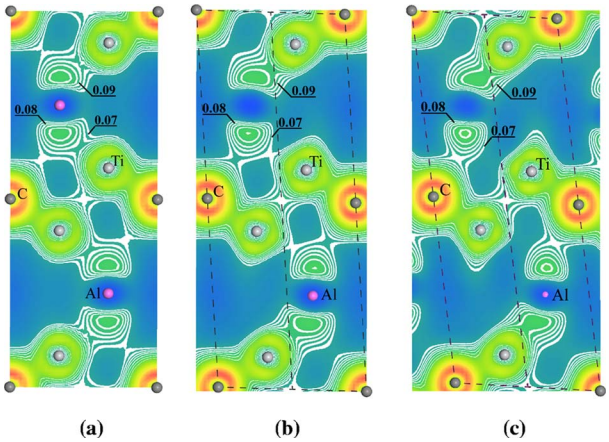

FIG. 5. (Color online) Distribution of valence electron density in a slice of $(11\bar{2}0)$ atomic plane of Ti_2AlC: (a) unstrained, (b) 0.1 shear strain, and (c) 0.2 shear strain.

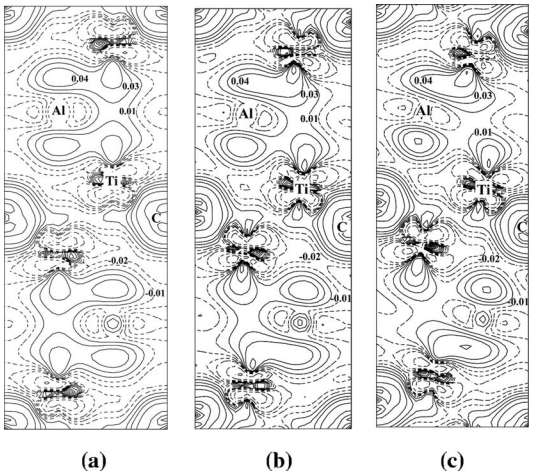

FIG. 6. Electron density difference in a slice of $(11\bar{2}0)$ atomic plane of Ti_2AlC: (a) unstrained, (b) 0.1 shear strain, and (c) 0.2 shear strain.

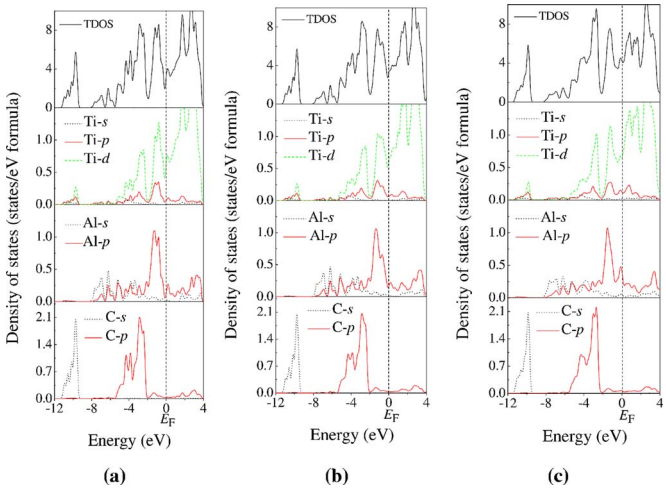

FIG. 7. (Color online) Total and projected density of states of Ti_2AlC (a) unstrained, and under shear strains of (b) 0.1, and (c) 0.2. The Fermi level is set as zero and marked by the vertical dashed line.

main stable. The shear deformation proceeds smoothly by bond softening rather than by an abrupt bond breaking of the Ti-Al bond. At shear strain of 0.2, the stretched Ti-Al bond reaches its limit of stability and breaks eventually. This leads to the gradual stress relaxation at large strains. Softening of the Ti-Al bond could be best understood from the extensive spatial distribution of p-derived orbitals of Al atoms. Therefore, the Al atoms can easily slip along the (0001) plane with small energy fluctuation. Once the shear strain energy is large enough to overcome a potential barrier, breakage of the weak Ti-Al covalent bond occurs and accounts for structural instability.

The electron density difference of shear-deformed Ti_2AlC is presented in Fig. 6 in order to illustrate the electron density arrangement. Accompanied with breaking of Ti-Al bonds, electron density accumulates along the $d(e_g)$ orbitals of Ti atoms. In contrast, half of the Ti-Al bonds are stable, but experience noticeable redistribution of valence electron density on the Ti $d(t_{2g})$-Al p bond.

Figure 7 shows the total and projected densities of states (DOS) of Ti_2AlC unstrained and under applied shear strains of 0.1 and 0.2. For the DOS of unstrained Ti_2AlC, a pseudogap at around −2.0 eV separates the two subgroups of valence bands. The states, which are approximately located between −5.8 and −2.0 eV below the Fermi level, originate from the bonding of Ti $3d$-C $2p$ orbitals. In more detail, states ranging from −5.8 to −3.4 eV corresponds to bonding of Ti $d(t_{2g})$-C p_z orbitals, and states extending from higher energy level, i.e., −2.8 to −2.0 eV, are dominated by Ti $d(t_{2g})-$C p_x/p_y bonding orbitals. The upper subgroup, which ranges from −2.0 eV to the Fermi level, composes of relatively weak Ti $d(e_g+t_{2g})$-Al p_z bonding orbitals. Furthermore, the peak of Ti $d(t_{2g})$-Al p_z bonding centers at low energy level, i.e., −1.3 eV, and the peak of Ti $d(e_g)$-Al p_z bonding centers at about −0.3 eV. States near and above the Fermi level are dominated by the Ti $d(e_g)$ orbitals. When examining the fine structures of DOS illustrated in Figs. 7(b) and 7(c), bonding stability under applied shear strain could be interpreted. The Ti $d(t_{2g})$-C p bonding states remain stable under the applied shear strain of 0.1, whereas, under the shear strain of 0.2, these states shift downward slightly, together with increments of peak height. The states shift away from the Fermi level by an average value of about −0.2 eV, which implies slight strengthening of Ti-C bonding. As illustrated in Fig. 6(c), valence electron density accumulates on the Ti $d(e_g)$-C p bonding orbitals, leading to the enhancement of bonding strength. The analysis of DOS characteristic of Ti-C bond demonstrates that Ti-C bond is very stable under shear deformation along the basal plane.

On the other hand, the Ti $d(e_g+t_{2g})$-Al p_z bonding states undergo significant changes under shear deformation. The peak of Ti $d(t_{2g})$-Al p_z bonding states shifts downward by −0.3 eV away from the Fermi level in Fig. 7(c), indicating a bond strengthening. In reinvestigating Fig. 6(c), the strengthening originates from the rearrangement of electron density on the Ti $d(t_{2g})$-Al p_z bonding. The peak of Ti $d(e_g)$-Al p_z bonding, in contrast, shifts upward as shown in Fig. 7(b), together with a noticeable decrease on peak height. This trend suggests that the Ti $d(e_g)$-Al p_z bonding is not favorable under the present studied symmetry-broken shear deformation. The valence electron density transfers from the Ti $d(e_g)$-Al p bond to the Ti $d(t_{2g})$-Al p_z bond as shown in Figs. 6(b) and 6(c). This rearrangement of electron density corresponds to the preserved Ti-Al bond under shear deformation. In Fig. 7(c), noticeable changes are the newly appeared DOS peak centering on −0.1 eV and enhancement of states at the Fermi level. These changes are induced by accumulation of electron density on the unbonded Ti $d(e_g)$ and Al p_z electronic states after the most stretched Ti-Al bond breaks. The present analysis shows that Ti-Al bonds are predominant to the low shear deformation resistance of ternary layered carbide and nitride. Also the result provides a mechanism for low hardness and intrinsic toughness of Al-contained ternary layered carbide and nitride.

For comparison, Figs. 8 and 9 show slices of valence electron density and electron density difference, respectively, in the (001) planes of a $2\times2\times1$ TiC supercell unstrained

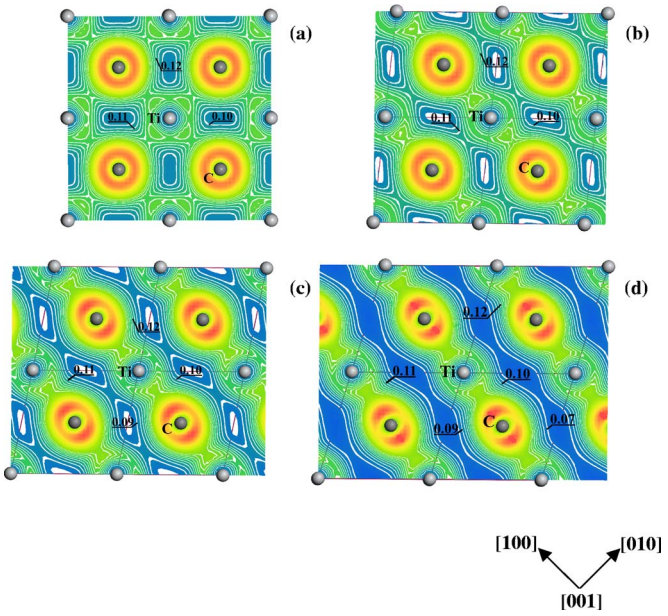

FIG. 8. (Color online) Distribution of valence electron density in a slice of (001) atomic plane of $2\times2\times1$ TiC supercell at various (110)[$\bar{1}$10] shear strains: (a) unstrained, (b) 0.1 shear strain, (c) 0.2 shear strain, and (d) 0.3 shear strain.

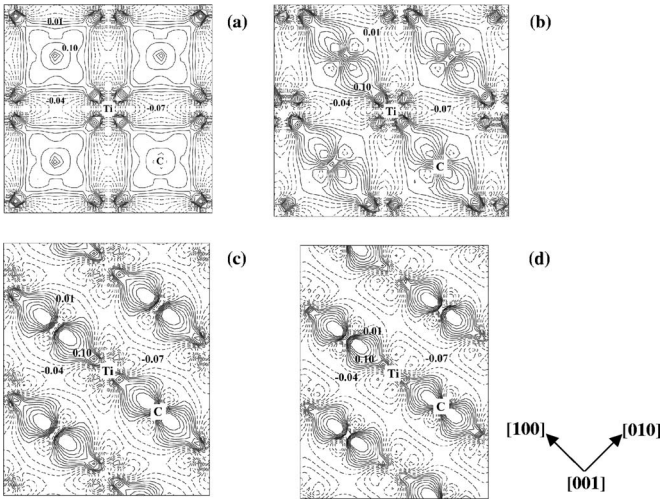

FIG. 9. Electron density difference in a slice of (001) atomic plane of $2\times2\times1$ TiC supercell at various (110)[$\bar{1}$10] shear strains: (a) unstrained, (b) 0.1 shear strain, (c) 0.2 shear strain, and (d) 0.3 shear strain.

and under (110)[$\bar{1}$10] shear deformation. In Figs. 8(a) and 9(a), Ti atoms bind to neighboring C atoms via $d(t_{2g})$-p σ-like bonding. Under applied shear deformation, the (110) atomic planes are strained in the [$\bar{1}$10] direction with the cubic symmetry broken. Meanwhile, as shown by Figs. 8(b), 8(c), 9(b), and 9(c), valence electron density along Ti-C bond depletes gradually on the (100) plane, and accumulates on the (010) plane. After the TiC lattice is shear deformed beyond the critical point of structural stability, such as under a strain of 0.25, bond breaking occurs on the (100) plane, as shown in Figs. 8(d) and 9(d). Since a [010] uniaxial tension can be regarded as a superposition of (110)[$\bar{1}$10] shear strain and an expansion perpendicular to the shear plane, the mechanism of failure reached by [010] tension is identical to that found by a (110)[$\bar{1}$10] shear. The structural instability occurs by similar bond-breaking events conducted by Ti-C bonds under tensile and shear deformations. Therefore, the ideal tensile and shear strengths show close values for binary compounds.

IV. CONCLUSION

We studied the deformation and failure modes of TiC, TiN, Ti_2AlC, and Ti_2AlN by using first-principles total-energy calculations. Different atomistic deformation modes are selected with considerations of experimental easy slip systems and crystal structural characteristics. It was found that the $TiC_{0.5}/TiN_{0.5}$ slabs remained structurally stable under deformations, whereas the weak Ti-Al bonds accommodated deformations by softening and breaking at large strains. The structural instability of ternary compounds was predominated by the shear slide of Al atomic planes along the basal plane.

The ideal stress-strain curves were presented and compared between binary and ternary compounds. The ideal shear strengths of ternary compounds were significantly smaller than those of the binary counterparts, whereas similar ideal tensile strengths were obtained. Low Vickers hardness was suggested as originating from low resistance to shear deformation for ternary compounds. The mechanism could be attributed to weak coupling between TiC_x/TiN_x slabs and Al atomic planes.

The electronic structural origin of deformation modes was analyzed and compared between binary and ternary compounds. The presence of weak Ti-Al bonds in ternary carbide and nitride weakened tensile strength by a small magnitude, whereas decreased the shear strength significantly. The extensive spatial distribution of Ti-Al bonds made shear deformation achieved easily without any abrupt bond-breaking events. Finally, the low shear deformation resistance was suggested the mechanism of damage tolerance and low hardness for ternary Al-containing carbides and nitrides.

ACKNOWLEDGMENTS

This work was supported by the National Outstanding Young Scientist Foundation for Y. C. Zhou under Grant No. 59925208, Natural Sciences Foundation of China under Grants No. 50232040, No. 90403027, and No. 50302011.

[1] B. R. Lawn, N. P. Padture, H. Cai, and F. Gurberteau, Science **263**, 1114 (1994).
[2] M. W. Barsoum, Prog. Solid State Chem. **28**, 201 (2000).
[3] J. Y. Wang and Y. C. Zhou, Phys. Rev. B **69**, 144108 (2004).
[4] J. Y. Wang and Y. C. Zhou, Phys. Rev. B **69**, 214111 (2004).
[5] J. Y. Wang and Y. C. Zhou, J. Phys.: Condens. Matter **16**, 2819 (2004).
[6] S. E. Lofland, J. D. Hettinger, K. Harrell, P. Finkel, S. Gupta, M. W. Barsoum, and G. Hug, Appl. Phys. Lett. **84**, 508 (2004).
[7] M. Šob, L. G. Wang, and V. Vitek, Kovove Mater. **36**, 145 (1998).
[8] W. Li and T. Wang, J. Phys.: Condens. Matter **10**, 9889 (1998).
[9] W. Luo, D. Roundy, M. L. Cohen, and J. W. Morris, Phys. Rev. B **66**, 094110 (2002).
[10] D. L. Price, B. R. Cooper, and J. M. Wills, Phys. Rev. B **46**, 11368 (1992).
[11] W. Li and T. Wang, Phys. Rev. B **59**, 3993 (1999).
[12] S. H. Jhi, S. G. Louie, M. L. Cohen, and J. W. Morris, Jr., Phys. Rev. Lett. **87**, 075503 (2001).
[13] M. D. Segall, P. L. D. Lindan, M. J. Probert, C. J. Pickard, P. J. Hasnip, S. J. Clark, and M. C. Payne, J. Phys.: Condens. Matter **14**, 2717 (2002).
[14] J. P. Perdew, J. A. Cherary, S. H. Vosko, K. A. Jackson, M. R. Pederson, D. J. Singh, and C. Fiolhais, Phys. Rev. B **46**, 6671 (1992).
[15] L. E. Toth, *Transition Metal Carbides and Nitrides* (Academic Press, New York, 1971), p. 153.
[16] L. Farber, M. W. Barsoum, A. Zavaliangos, and T. El-Raghy, J. Am. Ceram. Soc. **8**, 1677 (1998).
[17] M. W. Barsoum, L. Farber, and T. El-Raghy, Metall. Mater. Trans. A **30A**, 1727 (1999).
[18] For Ti_2AlN, TiC, and TiN, the elastic moduli are calculated in accordance with the same computational method of Ref. 4.
[19] M. W. Barsoum, M. Ali, and T. El-Raghy, Metall. Mater. Trans. A **31A**, 1857 (2000).
[20] D. G. Clerc and H. M. Ledbetter, J. Phys. Chem. Solids **59**, 1071 (1998).
[21] A. A. Ivan'ko, in *Handbook of Hardness Data*, edited by G. V. Samsonov (Keter Press, Jerusalem, 1971), p. 39.
[22] A. M. Kosevich, in *Dislocations in Solids*, edited by F. R. N. Nabarro (Amsterdam, North-Holland Publishing Company, 1979).
[23] Y. C. Zhou and Z. M. Sun, Mater. Res. Innovations **2**, 360 (1999).